Aerosol Science and Technology

ISSN: (Print) (Online) Journal homepage: https://www.tandfonline.com/loi/uast20

Computational and experimental study of aerosol dispersion in a ventilated room

George H. Downing, Yannis Hardalupas, Justice Archer, Henry E. Symons, Ulas Baran Baloglu, Daniel Schien, Bryan R. Bzdek & Jonathan P. Reid

To cite this article: George H. Downing, Yannis Hardalupas, Justice Archer, Henry E. Symons, Ulas Baran Baloglu, Daniel Schien, Bryan R. Bzdek & Jonathan P. Reid (2023) Computational and experimental study of aerosol dispersion in a ventilated room, Aerosol Science and Technology, 57:1, 50-62, DOI: 10.1080/02786826.2022.2145179

To link to this article: https://doi.org/10.1080/02786826.2022.2145179

Published online: 21 Nov 2022.

AEROSOL SCIENCE AND TECHNOLOGY
2023, VOL. 57, NO. 1, 50–62
https://doi.org/10.1080/02786826.2022.2145179

Computational and experimental study of aerosol dispersion in a ventilated room

George H. Downing[a], Yannis Hardalupas[a], Justice Archer[b], Henry E. Symons[b], Ulas Baran Baloglu[c], Daniel Schien[c], Bryan R. Bzdek[b], and Jonathan P. Reid[b]

[a]Department of Mechanical Engineering, Imperial College London, London, UK; [b]School of Chemistry, University of Bristol, Cantock's Close, Bristol, UK; [c]Department of Computer Science, University of Bristol, Bristol, UK

ABSTRACT

For many respiratory diseases, a primary mode of transmission is inhalation via aerosols and droplets. The COVID-19 pandemic has accelerated studies of aerosol dispersion in indoor environments. Most studies of aerosol dispersion present computational fluid dynamics results, which rarely include detailed experimental verification, and many of the computations are complex, making them hard to scale to larger spaces. This study presents a comparison of computational simulations and measurements of aerosol dispersion within a typical ventilated classroom. Measurements were accomplished using a custom-built low-cost sensor network composed of 15 commercially available optical particle sizers, which provided size-resolved information about the number concentrations and temporal dynamics of 0.3–40 μm diameter particles. Measurement results are compared to the computed dispersal and loss rates from a steady-state Reynolds-Averaged Navier–Stokes k-epsilon model. The results show that a newly developed aerosol-transport-model can accurately simulate the dispersion of aerosols and faithfully predict measured aerosol concentrations at different locations and times. The computational model was developed with scalability in mind such that it may be adapted for larger spaces. The experiments highlight that the fraction of aerosol recycled in the ventilation system depends on the aerosol droplet size and cannot be predicted by the recycled-to-outside air ratio. Moreover, aerosol recirculation is not negligible, as some computational approaches assume. Both modeling and measurements show that, depending on the location within the room, the maximum aerosol concentration can be many times higher than the average concentration, increasing the risk of infection.

ARTICLE HISTORY
Received 11 July 2022
Accepted 26 October 2022

EDITOR
Jing Wang

1. Introduction

The use of ventilation systems is prevalent in many areas of day-to-day life including in road vehicles, trains, airplanes, office buildings, and public places. Good ventilation is vital in maintaining good health, but current air quality regulations are not as developed as, for example, for food safety (Morawska et al. 2021). Wargocki indicated that health risks increase when the ventilation rate in homes is below 0.4 air changes per hour (ACH) (Wargocki 2013). Many high-rise and office buildings are now equipped with Heating, Ventilation and Air-Conditioning, (HVAC) systems, which control the movement of air within a building. HVAC systems use mechanical ventilation that utilizes fans and ducts to inject outside air and circulate room air, consuming a large amount of energy. HVAC systems currently consume around 12% of the worldwide final energy use (González-Torres et al. 2022). Air recirculation can be used to reduce the operating costs of HVAC systems, with some of the building air mixed with outside air from outside and resupplied to the room. Mixing of outside air with inside air already at temperature reduces the energy requirements for HVAC systems to heat or cool the ventilation air to a comfortable temperature (Göthe et al. 1988). However, such air recirculation increases the possibility that aerosols and contaminants can spread around a building.

With the COVID-19 pandemic, the dispersal and removal of aerosol within rooms and large spaces have become important topics of study. For many respiratory diseases, such as COVID-19 and influenza,

CONTACT George H. Downing g.downing20@imperial.ac.uk Department of Mechanical Engineering, Imperial College London, Exhibition Rd, South Kensington, London SW7 2BU, UK.

a dominant mode of transmission is via aerosols comprising liquid droplets (Wells and Stone, 1934; Sommerstein et al. 2020). The aerosol size distribution affects droplet dispersion in space, residence time in air, and deposition efficiency in the respiratory tract (Yhee, Im, and Nho 2016). For example, large droplet sizes (diameter $> 100\,\mu m$) tend to quickly sediment out of the air (i.e. seconds), whereas smaller aerosol droplets (diameter $< 100\,\mu m$) may remain airborne for long periods (i.e. hours) and may present greater infection risk (Prather et al. 2020). Moreover, viral load carried by droplets may depend on droplet size (Milton et al. 2013), highlighting the importance of aerosol dispersion due to airflow and its dependence on droplet size.

Computational modeling of aerosol dispersion in large spaces is challenging due to computational resource limitations, in particular when time-dependent computations are attempted in open spaces with complex geometries. The full range of timescales and lengthscales of the physics of airflow and aerosol droplet dispersion is impossible to resolve. Therefore, different assumptions are required to deliver computations that may provide an efficient and accurate prediction of aerosol dispersion physics. One modeling approach for aerosol transport is the use of a purely diffusive model, without any information of the local airflow characteristics, which uses the turbulent eddy diffusivity to provide enhanced diffusion due to turbulence. This technique has successfully been compared with experiments for both instantaneous and continuous release of aerosol for a variety of ventilation rates (Venkatram and Weil 2021). However, a shortfall of this method is that some dispersion characteristics cannot be captured if a significant convective flow is present in a room due to the ventilation duct placement resulting in an advection dominated regime. Additionally, this method does not account for varying aerosol droplet size.

Many studies of aerosol dispersion utilize computational fluid dynamics (CFD) and either are not evaluated by comparison with experiments (Hedworth et al. 2021; Mathai et al. 2021; Zhu et al. 2012; Gupta, Lin, and Chen 2011; Qian et al. 2009; Dbouk and Drikakis 2020; Dbouk and Drikakis 2020; Pendar and Páscoa 2020), or include minimal experimental verification (for example using a tracer gas of SF_6 to verify CFD results rather than aerosols) (Jiang et al. 2009) or use different fluids in an equivalent geometry (Poussou et al. 2010). Many studies do not investigate the dependence of dispersion on aerosol droplet size distribution, as such calculations can be computationally expensive. In addition, it is challenging to generate aerosols with wide size distributions and measure the transport and loss rates of particles of varying size in ventilated rooms. Therefore, understanding the dynamics of the size distribution of dispersed aerosols is crucial for the evaluation of disease transmission risk, and studies are required to robustly investigate the dependence of aerosol dispersal and loss on droplet size.

In this study, we aim to provide computational and experimental results for aerosol dispersion within a ventilated room and investigate the effect of particle size on dispersion. In particular, the effect of ventilation air recycling ratio on aerosol concentration decay rate is considered. We concentrate on particles smaller than $10\,\mu m$ diameter and will not consider the effect of evaporation in order to simplify the evaluation of the dispersion models. As droplet size has a large impact on aerosol dispersion, the potential impact of evaporation on dispersion cannot always be neglected and must be evaluated carefully. After exhalation, droplets can decrease significantly in size to around 20-40% of their initial diameter as they equilibrate with the ambient environment (Vejerano and Marr 2018). The time for full equilibration of a $10\,\mu m$ droplet can be around 1 s (de Oliveira et al. 2021). This short time is far less than the timescales of dispersion we are interested in this study. The effect of evaporation on the experiments was lessened by using a high weight percent of salt (20%) in the solution. This ensures that aerosol's dry diameter was still a significant portion of the initial wet diameter.

We present computational and experimental results for aerosol dispersion within a ventilated room. The inlet and outlet ventilation flowrates to the room were measured and used as inputs for the computational fluid dynamics (CFD) model. Aerosols were periodically generated in the room and their dispersion was measured experimentally using an array of low-cost sensors. Aerosol dispersion was simulated using a computational model that accounts for the local mean flow characteristics in the room and, with a modified aerosol-transport-model, the effects of turbulence on aerosol dispersion. The comparison between measurements and model predictions provide insight into how well a simplified computational model can represent aerosol dispersion in an indoor room environment and whether such an approach may be amenable to computational investigations of aerosol dispersion in larger scale environments (e.g. in buildings).

2. Methodology

This section presents the experimental arrangement and the tools that were used to obtain the measurements. It

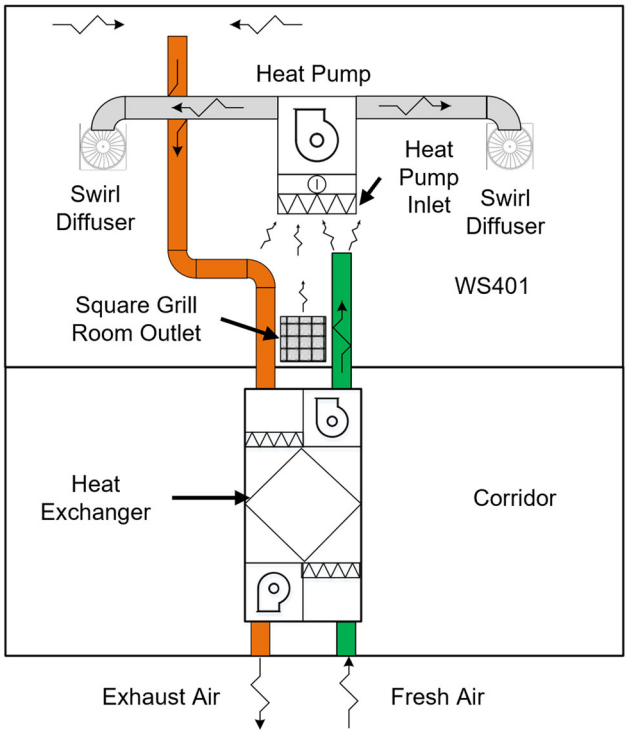

Figure 1. Top-down view of the false ceiling with ducting placement. Outside air flows into the false ceiling via the heat exchanger (green line) where is mixes with air being brought up from WS401 from the square grill. This mixed air is then drawn into the heat pump inlet where it enters WS401 via the swirl diffusers. The experimental room was WS401 in this diagram.

also presents the computational fluid dynamics models for the gas phase and the aerosol particles.

2.1. Experimental methods

2.1.1. Experimental room Set-Up

The test room used for the experiments and computational work was a typical classroom at the University of Bristol. The room is a cuboid with length 9.0 m, width 5.6 m and height 2.6 m. The room had desks and chairs (four of each) as well as three people working within, each wore a face mask. For all experiments the windows were kept shut, and door use was kept to a minimum to ensure an enclosed environment. Further measures were not taken as the amount of aerosol purposefully generated provided a sufficient signal above background noise. The room had two swirl diffusers in the ceiling that provided the ventilation air inlets, and one square grill in the ceiling for the ventilation outlet. The inlets were 56 cm in diameter and the outlet was 53 cm in length and width. Figure 1 shows the placement of the ventilation ducting in the ceiling of the test room (indicated by WS401 in the figure) and the adjoining corridor.

The total ventilation rate to the room was 11.3 air changes per hour (ACH), according to the room data sheet provided by the facilities management unit, and air flow measurements obtained with a hotwire probe at the square grill room outlet. The false ceiling of the room had a large void in which outside and recirculated air mixed, resulting in 7.5 ACH outside air drawn in from the outside with the remaining 3.8 ACH drawn as recycled air. We recognize that 11.3 ACH is a high flowrate, however this room was chosen for practicality and not because of the air-change rate. This air-change rate may have been different in other rooms and we did not have the opportunity to perform the experiment elsewhere. The fraction of aerosol recycled differs from the fraction of air recycled and is particle size dependent. Due to the placement of the square grill outlet adjacent to the inlet of the heat pump that feeds the swirl diffusers, it is conceivable that aerosols coming from the room to the ceiling void via this outlet may be recycled more easily than the air. The heat pump may also have some internal filters which will affect the amount of recycled aerosol. Initial assumptions are that all the aerosols (from outside air and recycled air) are filtered out and none are recycled, an assumption we shall revisit later in the discussion.

2.1.2. Aerosol generation

It was desirable to produce a high aerosol number concentration to resolve an increase in aerosol concentration relative to the background concentration. In addition, generation of a broad aerosol size distribution is desirable to quantify size dependent dispersion and loss rates. A typical 500 mL domestic mini snow mountain ultrasonic humidifier (SmartDevil) was used to generate 0.5–10.0 μm diameter particles from a 20-weight percent aqueous NaCl solution (water activity ~0.93 (Miyawaki et al. 1997)). The droplet size distribution generated by the humidifier (shown in Figure 2) was measured with an aerodynamic particle sizer (APS, TSI 3321, TSI Inc., Shoreview, MN) connected to the humidifier using 1 m of conductive silicon tubing in a straight line. The particles were released almost directly into the silicon tubing with the air outside the tubing being still. During transport from the humidifier to the APS only a portion of the aerosol would have fully evaporated, thus Figure 2 represents a distribution slightly larger than what would have been recorded by the low-cost sensor network. The effect of evaporation on the distribution was lessened by using a high weight percent of salt (20%) in the solution.

To generate short term responses from the low-cost aerosol sensors, the generator was operated for short periods of time ranging from 10-60 s. The duration of these pulses was recorded for use as inputs to the computational model. The generator was kept at the same position throughout all experiments (Figure 3).

2.1.3. Aerosol measurements

Aerosol number concentrations and size distributions (0.3—40 μm diameter) across the room were measured using a network of sensors consisting of 15 optical particle counters (Alphasense OPC N-3). The sampling frequency was 1 Hz. The uncertainty of the droplet concentration measurements of the optical particle counters has a maximum coincidence probability of 0.84% at 0.106 particles/cm^3 and 0.24% at 0.500 particles/cm^3. If the OPCs fluctuated between detecting particles and not (for example fluctuating between reporting 0 particles and 1 particle), then that size-bin was not used; this only happened for size bins greater than 10 μm for which the samples are limited by Poisson arrival statistics due to the low number concentration of larger aerosol particles. Analysis was therefore limited to droplet sizes less than 10 μm.

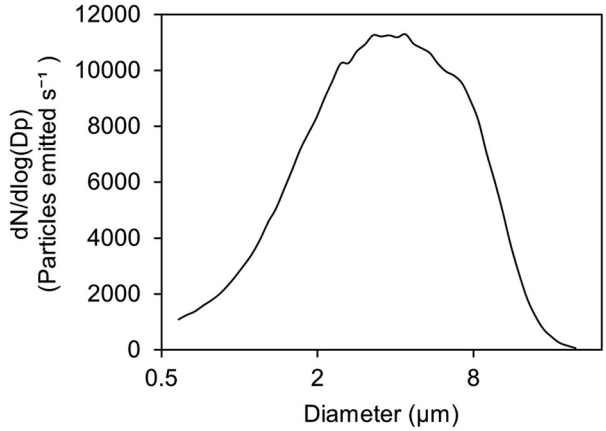

Figure 2. Droplet size distribution (measured by an APS) from the 500 mL humidifier, as measured close to the humidifier exit, so that the droplets had not evaporated.

Each optical particle counter was connected to a Raspberry Pi. The Raspberry Pis of all sensors were connected to an Intel NUC via Wi-Fi, allowing all the data from the network to be stored in a single location. The sensors were distributed across 10 pylons within the room. The positions are shown in Figure 3. The optical particle sizers were placed either at a height of 1.6 m (average height for the mouth when standing) or 1.2 m (average height for the mouth when sitting). All data were analyzed in a custom-written Python script. The data were smoothed by taking a rolling average of the previous 30 s of data. This one-sided averaging was preferred over centered averaging as it preserves the start time of pulses.

2.2. Computational methods

2.2.1. Fluid dynamics modelling

To compare experimental to computational results, a CFD model of the air flow in the room was created

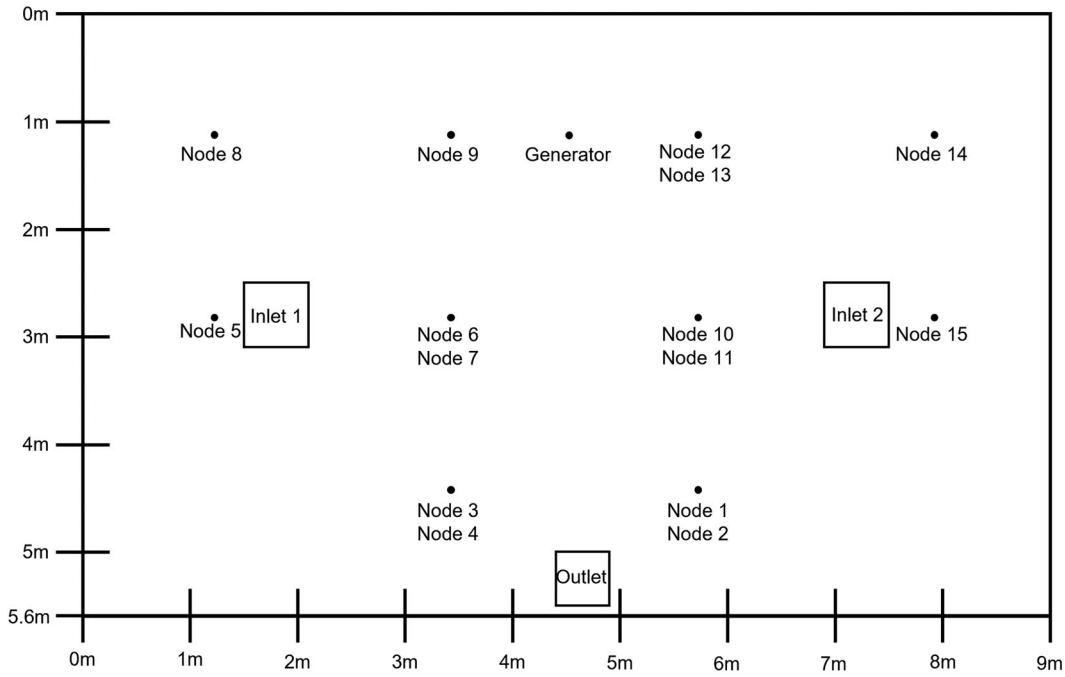

Figure 3. Top-down view of the room and sensor placements within the test room. All nodes are at a height of 1.6 m apart from Nodes 1, 3, 6, 10 and 12, which are at a height of 1.2 m. Diagram to scale.

using the OpenFOAM package (Weller et al. 1998). The room geometry was simplified as explained below to keep computational cost to a minimum. The computational room was set up as a cuboid with height 2.6 m and floor dimensions of 9.0 m by 5.6 m, closely matching the physical room. Internal features of the room, such as desks, chairs, and people, were not included in the computational domain.

The floor, ceiling and walls of the room were modeled as no-slip boundary conditions. The computational domain was divided into cells that were 10 cm in height, length and breadth. Two ventilation inlets and one outlet in the ceiling were modeled to represent the experimental room as closely as tractable. Although the square outlet has length and width of 53 cm, it was defined as a pressure outlet with a length and width of 60 cm to fit into the 10 cm cube cells. Air velocity measurements were obtained with a RS-8880 Hotwire Anemometer at different locations across the outlet, which provided a spatially averaged velocity that was multiplied by the outlet area to confirm that the outflow flowrate was 11.3 ACH (0.41 m^3 s^{-1}). The inlets to the room were two spiral diffusers which had an outer diameter of 56 cm and an inner diameter of 18 cm. The measured air velocity magnitude at the outer diameter was 6 m s^{-1}. In the computational domain, the inlets were modeled as a square annulus with a 60 cm outer diameter and a 20 cm inner diameter, such that it fitted into the 10 cm cells. The boundary conditions at the inlets were defined with a downward flowrate that would match the measured ACH, which led to a downward inlet area averaged velocity of 0.64 m s^{-1}. To match the measured velocity magnitude at the inlets, a rotational speed of 150 rpm in the clockwise direction (from top-down perspective) was added to the boundary conditions of the inlets.

The fluid flow within the room was calculated with a steady-state Reynolds-Averaged Navier–Stokes (RANS) k-epsilon model (Launder and Spalding, 1983). This computational method separates the velocity and pressure fields into a time-averaged (mean) component and a fluctuating component. The method then calculates the mean flow field and not the fluctuating velocity field, ensuring that a steady-state solution can be obtained. However, due to the non-linearity of the Navier–Stokes equations, the fluctuating field influences the mean field, resulting in a requirement for a turbulent closure problem. This non-linearity is treated by creating two extra fields, the turbulent kinetic energy (k) and the turbulent kinetic energy dissipation rate (epsilon (ϵ)). The turbulent

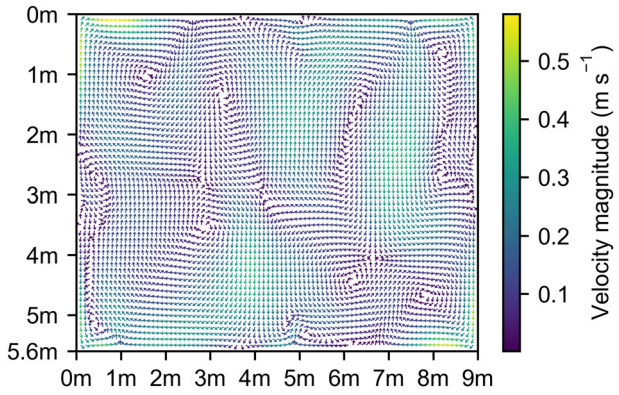

Figure 4. Top-down view of the velocity field at a height of 1.6 m. Grid size is 10 cm as seen in the figure and the velocity magnitude is according to the color scale in m s^{-1} (Figure 3 shows the room features for comparison).

kinetic energy is the square magnitude of the velocity fluctuations (given by Equation (1)) and, therefore, was quantified experimentally, and will be compared in the results section to the computations.

$$k = \frac{1}{2}\left(\overline{(u-\overline{u})^2} + \overline{(v-\overline{v})^2} + \overline{(w-\overline{w})^2}\right), \qquad (1)$$

where k is the turbulent kinetic energy, u, v, w are the velocities in the x, y and z directions respectively and the overbar represents a time average.

Figure 4 shows the top-down view of the grid size with the computed air flow at a height of 1.6 m across the room. The simulation used around 130,000 cells, which required 1 CPU hour to reach steady state, although availability of extra CPU cores will shorten the simulation time.

To evaluate the fluid flow simulation, the turbulent kinetic energy (TKE) was measured at several locations in the room and compared with the calculated turbulent kinetic energy from the CFD simulation at the equivalent locations in the computational domain. Turbulent kinetic energy was used as a guideline to assess the CFD simulation since it is an important parameter for the determination of the turbulent diffusion of aerosols (Equation (3)). Evaluation of the air flow velocities across the room was not undertaken due to the simplified room geometry in the computational domain. The turbulent kinetic energy was estimated from the measured velocity magnitude using a RS-8880 hotwire anemometer.

2.2.2. Aerosol modelling

Using a RANS k-epsilon model, it is possible to transport passive scalars (such as trace molecular concentrations). The mean convection velocity of the scalar is given by the mean air velocity field from the RANS calculations. The fluctuating velocity field of the air

flow also creates a fluctuating convection velocity of the scalar, which is often described as turbulent diffusion (Roberts and Webster 2002). The turbulent diffusion effect is often modeled as Fickian diffusion with a turbulent diffusivity. In the RANS k-epsilon model, the turbulent kinematic viscosity is given as (Launder and Spalding 1974):

$$\nu_t = C_\mu \frac{k^2}{\epsilon}, \tag{2}$$

where ν_t is the turbulent kinematic viscosity ($m^2\ s^{-1}$), C_μ is the dimensionless model coefficient for the turbulent viscosity with a default value of 0.09 that has been empirically fitted to several turbulent flows. k is the turbulent kinetic energy ($m^2\ s^{-2}$) and ϵ is the turbulent kinetic energy dissipation rate ($m^2\ s^{-3}$). To relate the turbulent kinematic viscosity with the turbulent diffusivity, a dimensionless turbulent Schmidt number is used (Brethouwer 2005):

$$Sc_t = \frac{\nu_t}{K}, \tag{3}$$

where Sc_t is the turbulent Schmidt number and K is the turbulent diffusivity ($m^2\ s^{-1}$). The simplest model for the turbulent Schmidt number, which has been used in this study, is to assume a constant value of $Sc_t = 1$.

Aerosols are not passive scalars, but have inertia and forces, such as weight and drag, which result in divergence from the fluid flow streamlines. The extent to which aerosols may divert from the fluid streamlines is quantified by the Stokes number (Brennen 2005):

$$Stk = \frac{\rho_p\ d_p^2}{18\ \mu_g}\ \frac{1}{t_f}, \tag{4}$$

where Stk is the Stokes number (dimensionless), ρ_p is the density of the aerosol particles ($kg\ m^{-3}$), d_p is the droplet diameter (m), μ_g is the dynamic viscosity of the gas (Pa s), and t_f is the fluid response time (s). ρ_p was assumed to be 2100 $kg\ m^{-3}$ for pure NaCl assuming the aerosol particles are fully dried to form crystalline particles (Lide 2004), justified by the measured 35% RH of the room. $\mu_g = 18.3\mu N\ s\ m^{-2}$ for air at 23 °C (Bearden 1939).

For $Stk \ll 1$, it can be assumed that the aerosol particles closely follow the fluid streamlines (Tropea et al. 2007). If the total mass of a particle is low, then momentum transfer from the particles to the fluid can be neglected with minimal error. Under these assumptions, aerosols can be assumed to act as passive scalars. Due to the difficulty of calculating the timescale t_f for the turbulent air flow, which may be different at different regions of the room, exact values of the Stokes numbers were not calculated. However, it was assumed that $Stk \ll 1$ due to the small size of particles (0.5 μm to 9.5 μm) and the low total mass of injected particles.

When modeling aerosol transport, the RANS mean velocity field was used for convection and the turbulent diffusivity for diffusion computations. It was assumed that turbulent diffusion would be far greater than any Fickian/molecular diffusion effects, thus these were not modeled. Since the experiments in the room lasted for a time scale of hours, the model also would have to simulate the aerosol transport for such a length of time.

Five micrometer salt particles have a terminal velocity in air of 5.6 $m\ h^{-1}$. With a room height of just 2.6 m, a significant number of aerosol particles might be expected to sediment out onto the floor over the course of an hour. As such, the mean velocities from the RANS model were adjusted for the calculation of aerosol convection, and an additional downward velocity that was equal to the terminal velocity of the particles was added to the RANS model to account for long-term sedimentation. The terminal velocity of the aerosol particles is defined as:

$$v_T = \frac{\rho_p\ d_p^2}{18\ \mu_g}\ g, \tag{5}$$

where v_T is the terminal velocity ($m\ s^{-1}$) and g is the gravitational acceleration of 9.81 $m\ s^{-2}$.

Modeling the aerosol transport as a passive scalar with convection and turbulent diffusion means that the dispersion properties are independent of the mean aerosol concentration up to a scaling factor, resulting in a free parameter when carrying out the simulations, which is the aerosol injection rate. The aerosol injection rate could be selected equal to the experimental injection rate. However, measuring the aerosol concentration by the generator could produce erroneous results as these particles may have only partially evaporated. As such a different method of estimating the aerosol injection rate within the simulation was chosen. The aerosol injection rate was chosen to be a fixed value so that the mean aerosol concentration of the experiment and the simulation matched.

Since any particle losses due to diffusion to the walls of the room were assumed negligible, the only particle losses were due to sedimentation or convection via the air flow vent. As discussed previously, the flow into the room consisted of a mixture of outside and recycled air. Using the experimental values of the recycle ratio of particles, described later, recycling of

air and particles was also implemented into the computational model to improve accuracy.

The aerosol transport model was custom written in Julia using the fluid flow results from OpenFOAM. The aerosol transport model used the same 130,000 cells as the CFD (Figure 4). Ten different aerosol particle sizes were tracked in the simulation for around 1 hour, requiring approximately 4 h of computational time using a graphics processor. With additional processing power, the different aerosol sizes could be simulated in parallel reducing the computational time.

The CFD and aerosol transport simulations were also repeated on 5 cm grid cells. Figure 5 shows there was a minimal difference in the number concentration profiles between the 5 cm (fine) and 10 cm (coarse) grids. Because computational and experimental results agree well, a 10-cm grid was used.

3. Results and discussion

3.1. Evaluation of fluid flow computation

The hotwire measurements are expected to underestimate the TKE, a consequence of the finite response time of the hotwire, which depends on the thickness of the wire; thicker wires 'filter out' higher frequency velocity fluctuations resulting in a lower magnitude estimate of TKE. As a result, we expect that the measured TKE to be systematically lower than the computed values from the CFD model. At the different room locations, the experimental TKEs were in the range of 3.2×10^{-3} to 9.4×10^{-3} m^2 s^{-2} and the computational TKEs were in the range of 5.2×10^{-3} to 1.1×10^{-2} m^2 s^{-2}, in line with expectations for slightly lower experimental TKEs than the CFD values to within an order of magnitude (around 60%).

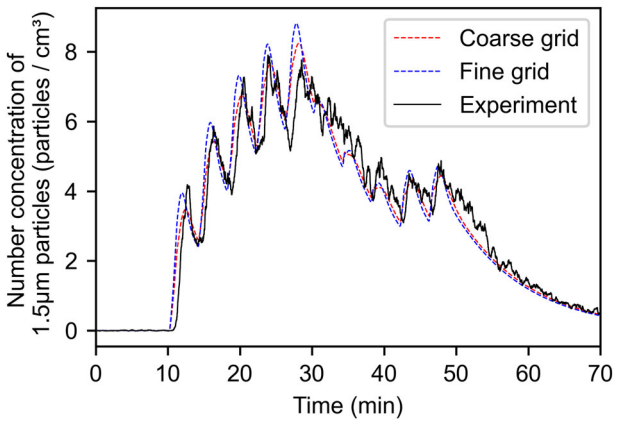

Figure 5. Time dependent aerosol particle number concentration computed at node 1 of a 5 cm grid (blue) and a 10 cm grid (red).

3.2. Aerosol characteristics

3.2.1. Model and experiment

The computations were compared to the aerosol concentration measurements at different locations and times within the room in order to assess the ability of the model to predict the dispersion of the aerosols. An experiment was designed that injected multiple sequential short pulses of aerosols that lasted for varying time lengths. Figure 6 shows the times when the aerosol generator was turned on and off during the experiment. The pulsed injection facilitates the detectors to observe the short timescale aerosol pulse dispersion due to diffusion and convection and the slow timescale decay of the aerosol due to droplet sedimentation and ventilation. After the pulsed aerosol injection, sufficient time is allowed for the aerosol concentrations to decay to background levels.

In total 165 different time series aerosol concentrations were recorded and analyzed using 15 different sensors, each with 11 size bins of useable data. Figure 7 reports the concentration of 2.0 μm particles recorded at nodes 12 and 1, which were located near the aerosol generator and far away, respectively. (See Figure 3 for the sensor placements.) Both the model (dashed lines) and experiment (solid lines) for node 12 (blue) show larger peaks than node 1 (red), and the time delay between the aerosol injection pulse and the measurement initiation by the detector is shorter for node 12, consistent with expectations since node 12 is closer. Good agreement can be seen between model and experimental results for both nodes. Remaining small differences between model and experiment can be accounted for when it is recognized that the model predicts average behavior whereas temporal changes to the instantaneous velocity field can cause large variations in the measured signal.

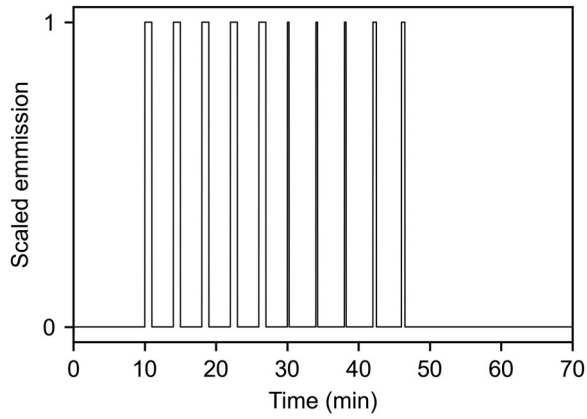

Figure 6. Aerosol injection pulses used in the experiment. 0 indicates the aerosol generator was switched off; 1 indicates the aerosol generator was switched on. The temporal sequence of the pulse included five 1-min pulses followed by three 15-s pulses and finally two 30-s pulses.

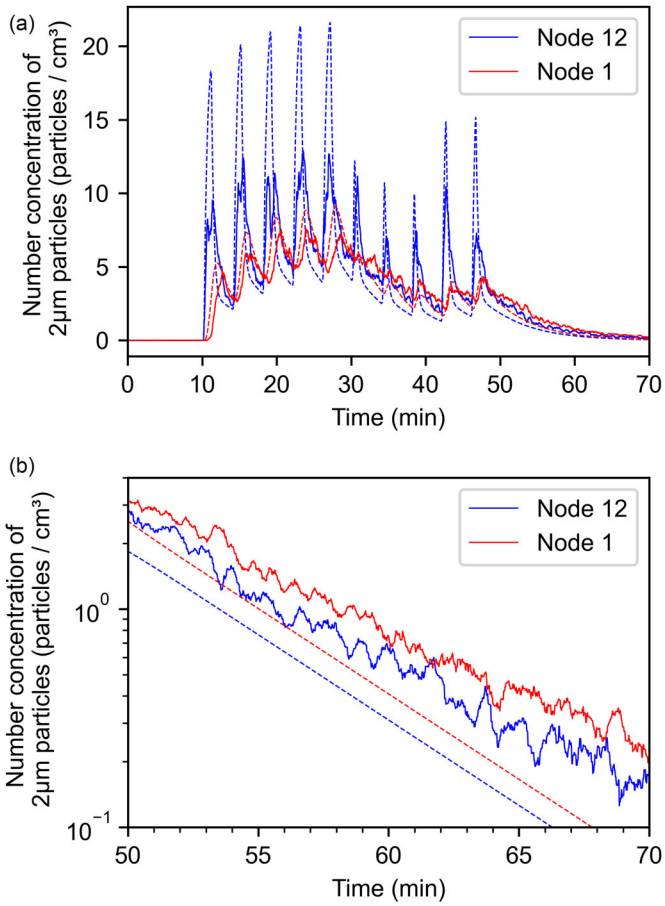

Figure 7. Model (dashed) and experimental (solid) temporal concentrations for 2.0 µm particles for Node 12 (placed near the aerosol generator, blue) and Node 1 (placed far from the aerosol generator, red). This model assumes no aerosol recirculation by the ventilation system. Model particle concentration rates were scaled by matching the mean of the model and experiment. (a) The full response and (b) the response after 50 min on a logarithmic scale.

The model predicts a faster decay rate of particle concentration than the experiment, as can be seen beyond 50 min. This first modeling approach did not allow recycling of particles through the ventilation duct and, thus, any aerosol particles leaving the room through the ventilation exhaust grid are permanently removed from the simulation.

3.2.2. Aerosol particle recycling

As discussed in the previous section, the model overpredicts the decay rate of 2.0 µm particles. One potential explanation for this observation is that some particles are recycled through the ventilation duct due to the placement of the outlet (Figure 1). To investigate the number of recycled particles, the aerosol generator was temporarily placed in the ceiling of the room near the exhaust vent and the amount of aerosol entering the room was measured using the sensor network. It was found that all particles greater than 5.85 µm were completely filtered, while varying amounts of smaller particles returned into the room.

An approach to quantify the amount of recycled aerosol particles in the room is to computationally calculate the decay rates and compare these to the experimental values. After around 2 min of aerosol injection, the particles become well-mixed in the room, and it can be assumed that the aerosol concentration is reasonably uniform throughout the room. By fitting an exponential decay to the data at the time that the aerosol is well-mixed across the room (specifically for the data after 55 min in Figures 7a and b), the size-dependent decay rate can be inferred and is reported in Figure 8.

Under a well-mixed assumption, a theoretical decay rate can be modeled taking into account the ventilation rate, the amount of recycled aerosol and the sedimentation rate of the aerosol. Diffusional losses of aerosol to the walls of the room are neglected in this simple model as it is assumed that turbulent diffusion approaches zero in the laminar boundary layer of the walls and particle Brownian diffusion is insignificant for the considered sizes of aerosol particles (>0.5 µm). The sedimentation rate of the aerosol was taken to be

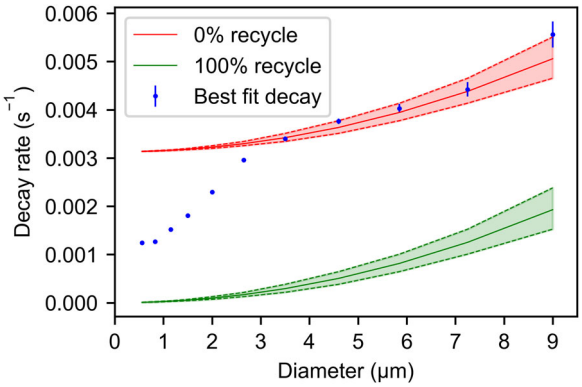

Figure 8. Experimental decay rates (blue) along with theoretical decay rates assuming 0% recycled particles (red, solid) and 100% recycled particles (green, solid) for different particle sizes. The error bar of the experimental data represents the standard error of the exponential fit. The error in the theoretical decay rates (distance between the two dashed lines) represents the width of the bin size of the low-cost sensors.

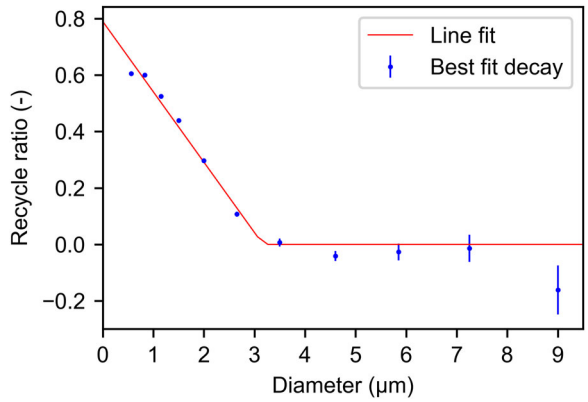

Figure 9. Calculated recycling ratios (blue) as a function of particle size based on results of Figure 8, and best fit line (red) used in the computations with the Experimentally Informed CFD Model. Arrow heads represent the uncertainty. For the linear portion $r^2 = 0.97$.

the terminal velocity of the particle multiplied by the floor area and the aerosol concentration. The derived equation for the decay is given below as:

$$\frac{dC}{dt} = -\frac{\left(Q(1-R) + v_T A_{floor}\right)}{V_{room}} C, \qquad (6)$$

where C is the well-mixed aerosol concentration in the room (m^{-3}), t is time (s^{-1}), Q is the total ventilation rate of the room (0.41 m^3 s^{-1}), R is the recirculation ratio of particles in the ventilation system (unitless), v_T is the particle terminal velocity given by Equation (5) (m s^{-1}), A_{floor} is the total floor area of the room (50.4 m^2), and V_{room} is the volume of the room (131 m^3).

The theoretical decay rate for 100% recycled aerosol ($R = 1$ in Equation (6), green) and 0% recycled aerosol ($R = 0$ in Equation (6), red) is shown in Figure 8 for different particle sizes. The simulations and experiments reported in Figure 8 are consistent with the measurements with the aerosol source positioned in the ceiling with large aerosol particle sizes well described when assuming no recycling of aerosol (red). However, the experimental data show significant deviation from this line for small particle sizes, also consistent with the ceiling experiment and substantial recycling of small particles into the room.

By using Figure 8, it is possible to estimate the recycle ratio of aerosol based on the decay rate model (Equation (6)), which is presented in Figure 9. A line (red) was fitted to the calculated recycling ratios using Equation (6) (blue crosses) and, as expected, the amount of recycled aerosol increases as the particle size decreases since smaller particles more efficiently pass through the ventilation filter. An important consequence of Figure 9 is that the decay rate of aerosols cannot be simply predicted by using the air changes of the room. The CFD flow field may be recalculated using these recycling ratios to deliver an experimentally informed model, as seen in the next section.

3.2.3. Experimentally informed computational model

The flow field was recalculated using the experimentally determined recycling ratios plotted in Figure 9. The results from the revised model for 2.0 μm particles at nodes 1 and 12 are presented in Figures 10a and b, which can be compared directly to the results of the model that ignores recirculation (see Figure 7). This comparison shows that the model with recirculation of aerosol matches the experimental data much better than the model without recirculation, especially in the time region after 55 min. The experimentally informed model predicts a slower decay rate of aerosol particle concentration due to the recycled aerosol.

Figure 11 shows the effect of aerosol size on aerosol dispersion in the room. Figure 11a shows the temporal response for the concentration of 1.5 μm particles and Figure 11b that of 7.25 μm particles. For 7.25 μm particles, the aerosol concentration does not rise as much compared to the 1.5 μm particles due to the slower decay rates of 1.5 μm particles and fewer 7.25 μm generated.

Aerosol mass concentration is a key parameter used to quantify air quality. Figure 12 shows the measured PM_{10} (total particle mass of all particles less than 10 μm in diameter) temporal responses across the low-cost sensor network and the comparison to model predictions. When comparing aerosol concentrations between experiment and simulation there are two types of error to consider, these are temporal errors and concentration errors. Quantitative assessments of the accuracy of the

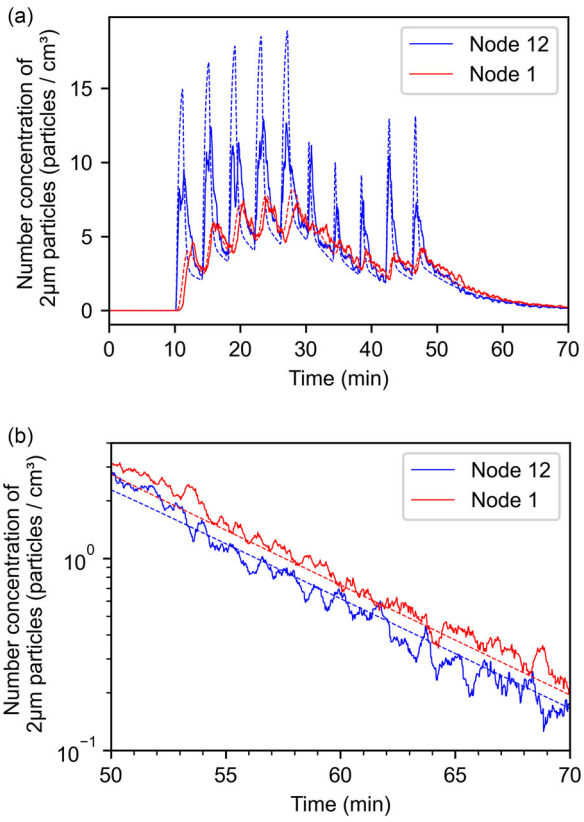

Figure 10. Model (dashed) and experimental (solid) temporal responses for the concentration of the 2.0 μm particles for Node 12 (blue) and Node 1 (red). This model uses the recycling ratios defined in Figure 8. Model and experimental values were scaled together by matching their median values. (a) Shows the full response (b) Shows the response after 50 min on a logarithmic scale.

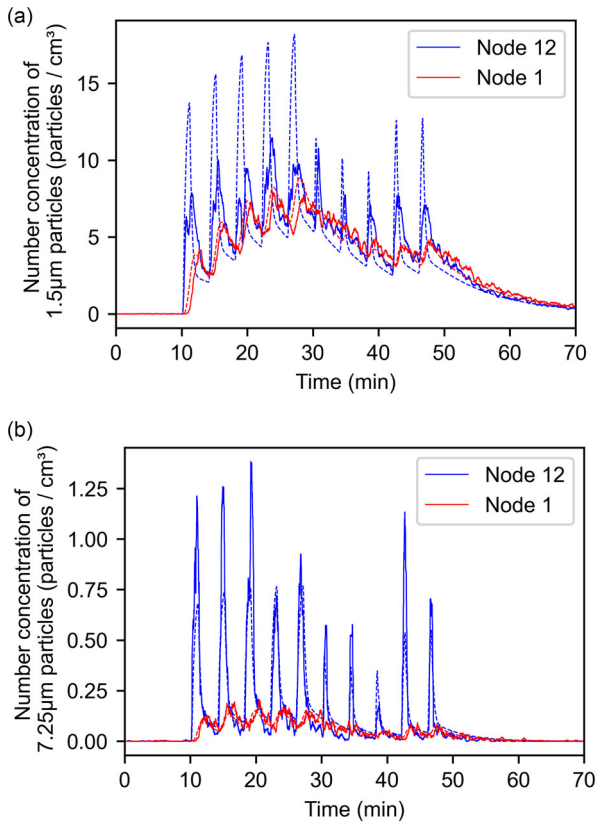

Figure 11. Time-dependent experimental measurements (solid) and model predictions (dashed) of aerosol number concentration at Node 12 (blue) and Node 1 (red) for (a) 1.5 μm and (b) 7.25 μm particles.

simulations have not been undertaken as it would mean assigning a weight to these two errors. However, it is still possible to draw conclusions from these data by qualitatively comparing the location and strength of the pulses and their decays. We observe very good agreement between model and experiment for all sensors; both long-term decay rate and short-term diffusion of the aerosol are well captured for all measurement nodes and the duration of the pulses causing different magnitude peaks is also well captured. There are four locations, which show the worst temporal and pulse strength match between model and experiments, which are nodes 6, 7, 10 and 11. These nodes are located at the center of the room (Figure 3) where the two large airflow vortical structures, generated from the inlet swirl diffusers, interact. It is not surprising that this location has the lowest agreement with experimental data since the simplicity of the CFD calculation does not capture the complexity of the local flow. The mixing at this central region of the airflow is perhaps not captured well by a RANS *k*-epsilon model. However, it is more likely that this is caused by the lack of some geometrical features of the room in the computational domain, which existed in the experiment such as tables and chairs. Another area of interest are nodes 3, 4 and 5 compared to their counterparts 1, 2 and 15. The left-hand side of the room (Figure 3) has worse agreement with experimental results than the right-hand side. This could be due to the slight off-center outlet (Figure 3) or more likely the combined rotational velocities of both diffusers being better captured on the right hand side.

3.3. Discussion

When experimental data are used to inform the computational model on the recycling ratios in the room from the ventilation system, the agreement between model and experiments is very good in both space and time (Figure 12). This provides evidence that the proposed simplified approach for the CFD calculation of the air flow and aerosol transport is sufficient to predict aerosol transport in large spaces, at least as large as the room size of the current study. From our results, we see that proximity to the initial aerosol injection event results in extreme maximum aerosol

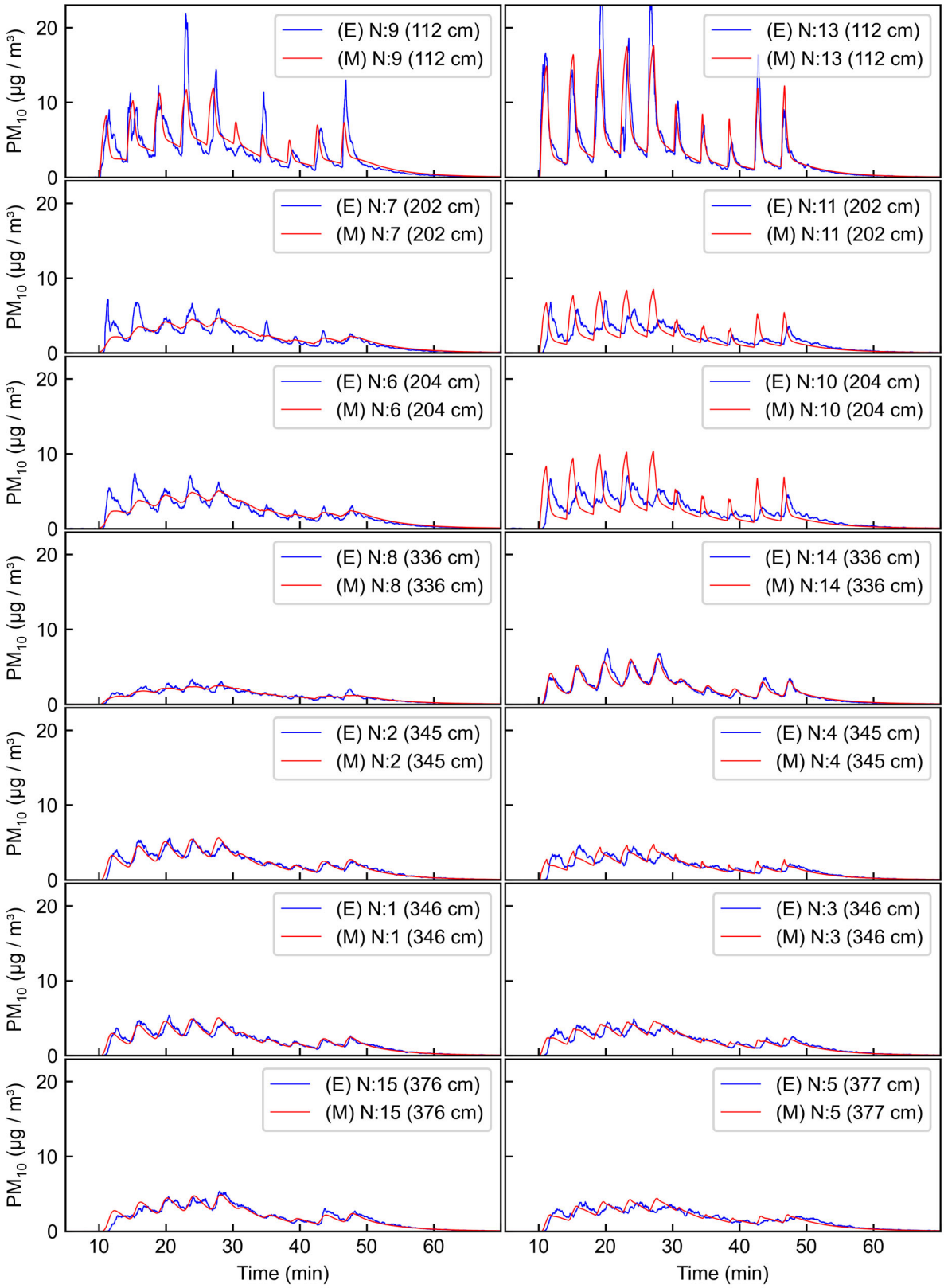

Figure 12. Showing PM_{10} for all nodes (except Node 12). Nodes are ordered based on distance from the aerosol generator. Blue (E) lines are the experimental values, orange (M) lines are the CFD model with recycling. All graphs have the same axis scales.

exposure that quickly dissipates. A more surprising result is the amount of time that aerosols reside in the room. For a ventilation rate of 11.3 ACH, it takes around 30 min for concentration levels of 2 µm to reach 5% of the peak (based on decay rate in Figure 8), and therefore everyone in the room would

have significant exposure to the initial aerosol injection event. This is longer than what simple calculation would predict, and this behavior could provide better models for exposure and disease transmission risks. However, it is noted that the experimentally evaluated recycling ratio depends on the geometry of the room and the ventilation system and this evaluation must be repeated for different geometries.

Many existing computational studies of aerosol transport do not investigate the effect of particle size on aerosol transport. Figures 8 and 11 demonstrate that particle size has a significant effect on dispersion and decay rates. Consequently, the effect of particle size should not be neglected in computational models. In our experimental setup, there are two reasons for the large differences between the behavior of different aerosol particle sizes. Under a fixed ventilation rate, aerosol dispersion for particle diameters greater than 3 μm is dominated by the varying sedimentation rate with size (Figure 8). However, for diameters less than 3 μm, the variable recycling rates of aerosols in the ventilation ducting accounts for the large variation in the aerosol dispersion for different particle sizes. There is no simple way to estimate aerosol recycling ratios without an experimental measurement. Based on pure airflow measurements, we might expect all aerosols to have a recycling ratio of $R = 0.34$, (7.5 ACH outside air, 11.3 ACH total ventilation). However, based on Figure 9, the recycling ratios of aerosols for this room vary between $R = 0.6$ and $R = 0.0$ depending on particle size. By observing Figure 1, it is possible to reason that most of the aerosol is expected to enter the heat pump inlet due to the placement of the room outlet. In hindsight, this is a poor design in terms of aerosol filtration as it allows higher recycling of aerosol than air. The decline of the recycling ratio of aerosol down to $R = 0.0$ is most likely due to some internal filtration in the heat pump unit, however no specifications for the heat pump were found. This lack of specification is common for most ventilation systems, as manufacturers do not need to provide detailed filtration specifications. These results provide significant conclusions for future aerosol dispersion CFD modeling, indicating that any simulations performed without experimental verification or extensive filtration and ventilation information may be invalid. This size dependent recycle is unlikely to be significant for rooms with industrial ventilation with HEPA filters, but, for typical rooms, such as workspace offices and classrooms, this effect should not be ignored.

Subsequent work should focus on applying and verifying this combined experimental and modeling approach to other test rooms, such as larger rooms with more complex ventilation arrangements. Our approach was computationally efficient due to the steady velocity calculation and the simplicity of the aerosol transport model. Thus, it is well suited for spaces even larger than the room of the current study, and as the transport of aerosol is largely dominated by turbulent diffusion, high resolution in the velocity is not required. Additional work could develop a disease transmission risk based on the room and exposure times, evaluating the effectiveness of practices such as the 2-m rule. More research should be performed to consider different ventilation rates, assessing the effectiveness of reducing aerosol dispersion and exposure. Finally, to reduce the computational costs and simplify the analysis, we assumed that the aerosol was already dry with no diameter change due to evaporation. Aerosol generated by vocalization contain water and salts and undergo some evaporation upon initial discharge depending on particle size and RH. As such the experiment should also be repeated with lower salt concentrations and the computations repeated with evaporation included.

4. Conclusions

A combined experimental and computational approach has been developed to predict aerosol dispersion around a room. It is possible to predict the temporal and spatial aerosol concentrations within the room for different particle sizes with good accuracy. The results show that depending on location within the room the peak concentration of aerosol can be many times more than the average concentration. Additionally, depending on room layout, the number of air changes per hour may not be representative of the decay rate of aerosol particles, as they may be recycled, and this recycling ratio depends on size. This shows that the number of air changes per hour is an insufficient metric for determining the safety of a room in terms of disease transmission unless additional information about air filtration is known. This study also shows that modeling aerosols as a pure scalar is insufficient for large particles because over long times (hours), sedimentation can play a major role.

Funding

The authors acknowledge funding from the Engineering and Physical Sciences Research Council (EP/V050516/1) and the UK Collaboratorium for Research in Infrastructure & Cities: Urban Observatories (Strand B) (EP/P016782/1). B.R.B. acknowledges the Natural Environment Research Council (NE/P018459/1). The authors also acknowledge the Center for Doctoral Training in Aerosol Science, which supports G.D. through grant EP/S023593/1.

Data availability statement

Data are available at the Imperial College London data repository at https://doi.org/10.14469/hpc/11195.

References

Bearden, J. A. 1939. A precision determination of the viscosity of air. *Phys. Rev.* 56 (10):1023–40. doi:10.1103/PhysRev.56.1023.

Brennen, C. E. 2005. *Fundamentals of multiphase flow*. Cambridge: Cambridge University Press.

Brethouwer, G. 2005. The effect of rotation on rapidly sheared homogeneous turbulence and passive scalar transport. Linear theory and direct numerical simulation. *J. Fluid Mech.* 542 (1):305–42. doi:10.1017/S0022112005006427.

Dbouk, T., and D. Drikakis. 2020. On coughing and airborne droplet transmission to humans. *Phys. Fluids (1994)* 32 (5):053310. doi:10.1063/5.0011960.

Dbouk, T., and D. Drikakis. 2020. Weather impact on airborne coronavirus survival. *Phys. Fluids (1994)* 32 (9):093312. doi:10.1063/5.0024272.

de Oliveira, P. M, et al. 2021. Evolution of spray and aerosol from respiratory releases: theoretical estimates for insight on viral transmission. *Proc R. Soc A* 477(2245):20200584.

González-Torres, M., L. Pérez-Lombard, J. F. Coronel, I. R. Maestre, and D. Yan. 2022. A review on buildings energy information: Trends, end-uses, fuels and drivers. *Energy Rep.* 8:626–37. doi:10.1016/j.egyr.2021.11.280.

Göthe, C. J., R. Bjurström, and K. Ancker. 1988. A simple method of estimating air recirculation in ventilation systems. *Am. Ind. Hyg. Assoc. J.* 49 (2):66–9. doi:10.1080/15298668891379404.

Gupta, J. K., C. Lin, and Q. Chen. 2011. Transport of expiratory droplets in an aircraft cabin. *Indoor Air.* 21 (1):3–11. doi:10.1111/j.1600-0668.2010.00676.x.

Hedworth, H. A., M. Karam, J. McConnell, J. C. Sutherland, and T. Saad. 2021. Mitigation strategies for airborne disease transmission in orchestras using computational fluid dynamics. *Sci. Adv.* 7 (26):eabg4511. doi:10.1126/sciadv.abg4511.

Jiang, Y., B. Zhao, X. Li, X. Yang, Z. Zhang, and Y. Zhang. 2009. Investigating a safe ventilation rate for the prevention of indoor SARS transmission: An attempt based on a simulation approach. *Build. Simul.* 2 (4):281–9. doi:10.1007/s12273-009-9325-7.

Launder, B. E., and D. B. Spalding. 1974. The numerical computation of turbulent flows. *Comput. Methods Appl. Mech. Eng.* 3 (2):269–89. doi:10.1016/0045-7825(74)90029-2.

Launder, B. E, and D. B. Spalding. 1983. The numerical computation of turbulent flows. *In: Numerical Prediction of Flow, Heat Transfer, Turbulence and Combustion*. ed. S. V. Patankar, A. Pollard, A. K. Singhal, and S. Pratap Vanka, 96–116. London: Pergamon.

Lide, D. R. 2004. *CRC handbook of chemistry and physics*. Boca Raton, FL: CRC press.

Mathai, V., A. Das, J. A. Bailey, and K. Breuer. 2021. Airflows inside passenger cars and implications for airborne disease transmission. *Sci. Adv.* 7 (1):eabe0166. doi:10.1126/sciadv.abe0166.

Milton, D. K., M. P. Fabian, B. J. Cowling, M. L. Grantham, and J. J. McDevitt. 2013. Influenza virus aerosols in human exhaled breath: particle size, culturability, and effect of surgical masks. *PLoS Pathog.* 9 (3):e1003205. doi:10.1371/journal.ppat.1003205.

Miyawaki, O., A. Saito, T. Matsuo, and K. Nakamura. 1997. Activity and activity coefficient of water in aqueous solutions and their relationships with solution structure parameters. *Biosci. Biotechnol. Biochem.* 61 (3):466–9. doi:10.1271/bbb.61.466.

Morawska, L., J. Allen, W. Bahnfleth, P. M. Bluyssen, A. Boerstra, G. Buonanno, J. Cao, S. J. Dancer, A. Floto, F. Franchimon, et al. 2021. A paradigm shift to combat indoor respiratory infection. *Science* 372 (6543):689–91.

Pendar, M.-R, and J. C. Páscoa. 2020. Numerical modeling of the distribution of virus carrying saliva droplets during sneeze and cough. *Phys. Fluids (1994)* 32 (8):083305. doi:10.1063/5.0018432.

Poussou, S. B., S. Mazumdar, M. W. Plesniak, P. E. Sojka, and Q. Chen. 2010. Flow and contaminant transport in an airliner cabin induced by a moving body: Model experiments and CFD predictions. *Atmos. Environ.* 44 (24):2830–9. doi:10.1016/j.atmosenv.2010.04.053.

Prather, K. A., L. C. Marr, R. T. Schooley, M. A. McDiarmid, M. E. Wilson, and D. K. Milton. 2020. Airborne transmission of SARS-CoV-2. *Science* 370 (6514):303–4.

Qian, H., Y. Li, P. V. Nielsen, and X. Huang. 2009. Spatial distribution of infection risk of SARS transmission in a hospital ward. *Build. Environ.* 44 (8):1651–8. doi:10.1016/j.buildenv.2008.11.002.

Roberts, P. J., and D. R. Webster. 2002. *Turbulent diffusion*. Reston: ASCE Press.

Sommerstein, R., C. A. Fux, D. Vuichard-Gysin, M. Abbas, J. Marschall, C. Balmelli, N. Troillet, S. Harbarth, M. Schlegel, A. Widmer, et al. 2020. Risk of SARS-CoV-2 transmission by aerosols, the rational use of masks, and protection of healthcare workers from COVID-19. *Antimicrob. Resist. Infect. Control* 9 (1):1–8. doi:10.1186/s13756-020-00763-0.

Tropea, C., A. L. Yarin, and J. F. Foss. 2007. *Springer handbook of experimental fluid mechanics*. 1 ed. Berlin: Springer.

Vejerano, E. P, and L. C. Marr. 2018. Physico-chemical characteristics of evaporating respiratory fluid droplets. *J. R Soc. Interface* 15 (139):20170939. doi:10.1098/rsif.2017.0939.

Venkatram, A, and J. Weil. 2021. Modeling turbulent transport of aerosols inside rooms using eddy diffusivity. *Indoor Air* 31 (6):1886–95. doi:10.1111/ina.12901.

Wargocki, P. 2013. The Effects of Ventilation in Homes on Health. *Int. J. Vent.* 12 (2):101–18. doi:10.1080/14733315.2013.11684005.

Weller, H. G., G. Tabor, H. Jasak, and C. Fureby. 1998. A tensorial approach to computational continuum mechanics using object-oriented techniques. *Comput. Phys.* 12 (6):620–31. doi:10.1063/1.168744.

Wells, W. F., and W. R. Stone. 1934. On Air-borne Infection. Study III. Viability of Droplet Nuclei Infection. *Am. J. Hygiene* 20 (3):619–27. doi:10.1093/oxfordjournals.aje.a118098.

Yhee, J. Y., J. Im, and R. S. Nho. 2016. Advanced therapeutic strategies for chronic lung disease using nanoparticle-based drug delivery. *JCM.* 5 (9):82. doi:10.3390/jcm5090082.

Zhu, S., J. Srebric, J. D. Spengler, and P. Demokritou. 2012. An advanced numerical model for the assessment of airborne transmission of influenza in bus microenvironments. *Build. Environ.* 47:67–75. doi:10.1016/j.buildenv.2011.05.003.